Pergamon

Acta mater. Vol. 45, No. 10, pp. 4297–4309, 1997

PII: S1359-6454(97)00075-X
1359-6454/97 $17.00 + 0.00

Al–4 wt% Cu COMPOSITE REINFORCED WITH IN-SITU TiB_2 PARTICLES

L. LU, M. O. LAI and F. L. CHEN

Department of Mechanical and Production Engineering, National University of Singapore, 10 Kent Ridge Crescent, Singapore 119260

(Received 6 August 1996; accepted 18 December 1996)

Abstract—Al–4 wt% Cu/TiB_2 metal matrix composite has been fabricated with an exothermic reaction process at 850°C via K_2TiF_6 and KBF_4 salts. Microstructural observation revealed the hexagonal shape of the in-situ TiB_2 particles after a reaction holding time of 5 min. Although the exothermic reaction became more nearly complete with the increase in reaction time, the size of the in-situ TiB_2 particles was less dependent on reaction time. Microstructural observation showed that the grain size of the composite was refined dramatically at the beginning of the reaction. However, it increased slightly at the later stage of the reaction. Because of the change in the volume of TiB_2 and grain size, the yield and ultimate tensile stresses of the composite increased with reaction durations. Fractographs of the in-situ metal matrix composite showed ductile fracture mode. © *1997 Acta Metallurgica Inc.*

1. INTRODUCTION

The Orowan strengthening mechanism requires very fine reinforcement particles in the range of 500 nm homogeneously dispersed as the secondary phases within the matrix [1]. The particles should be well bonded with the matrix, with no debonding between particles and the matrices during the motion of dislocations. Currently, most processes employed in synthesis of metal matrix composites (MMCs) involve the incorporation of ceramic particles, such as SiC, into the matrices via casting and powder metallurgy methods. The major drawback in the former process involves the difficulties encountered in incorporating the fine ceramic reinforcements into the matrices, agglomeration and poor wetting between particles and matrices. If SiC particles are incorporated into a silicon-free melt, the particles are thermodynamically unstable and form aluminium carbide with the Al melt:

$$4Al + 3SiC = Al_4C_3 + 3Si. \quad (1)$$

This reaction leads to a decrease in mechanical, physical and chemical properties because of the brittleness of the Al_4C_3 phase, and its water reactivity. Owing to the above reaction between Al melt and SiC, the amount of SiC decreases. A higher percentage of Si content is therefore required to be added in the melt to prevent the decomposition of SiC.

To counteract this problem and to increase the bonding strength between the particles and the matrix, Lanxide™ and XD™ in-situ composite materials have been developed [2]. The use of these materials, which involves exothermic synthesis, has received new attention as a better way of producing in-situ ceramic particles in the fabrication of Al-based alloys [3–5]. Different reinforcements of TiC, TiN, TaC, SiC, etc., have been in-situ synthesized using Lanxide™, XD™, self-propagation high temperature (SHS) [6] and reactive gas injection [7]. One breakthrough reported is flux assisted synthesis of MMCs as patented by Davies *et al.* [8]. In this synthesis, molten salts are introduced into an aluminium melt. A chemical reaction between the salts and the molten aluminium takes place to form TiB_2 particles *in situ*. The major advantage of this in-situ process is that the dispersoid TiB_2 is created by the reaction so that the particles are formed within the melt and there is less problem with distribution of the in-situ particles. Since the MMCs produced in-situ are under near-equilibrium conditions, they generally possess low energy interphase boundaries, indicating that they are intrinsically stable [9]. For the conventional synthesis of MMCs by introducing particles into the matrix, however, unclear particle surfaces, non-uniform distribution of particles and settling of particles during casting can generally be observed in the final products. Some investigations carried out by using Ti, B and Al powders heated together to 800°C to form in-situ TiB_2 have been reported [10, 11].

The formation of TiB_2 in a melt is an exothermic process where the chemical reaction occurs according to the following sequence [12]:

$$K_2TiF_6 + Al \Rightarrow TiAl_3 + KAlF_4 + K_3AlF_6 \quad (2)$$

$$KBF_4 + Al \Rightarrow AlB_2 + KAlF_4 \quad (3)$$

and

$$AlB_2 + TiAl_3 \Rightarrow TiB_2 + Al. \quad (4)$$

The maximum amount of TiB_2 formed *in situ* is determined by the viscosity of the subsequent melt. Values of up to 12% have been reported [12].

Several different reactions have been proposed between Al, Ti and B. Maxwell and Hellawell [13] suggested a ternary peritectic reaction of L (liquid) + $TiAl_3$ + TiB_2 ↔ (Al) above 665°C and a ternary eutectic reaction of L ↔ (Al) + TiB_2 + AlB_2 below 659°C. However, Abdel-Hamid and Durand [14] proposed two transition reactions of L + $TiAl_3$ ↔ (Al) + TiB_2 and L + TiB_2 ↔ (Al) + AlB_2 occurring within the temperature range 665–659°C. A thermodynamic calculation [15, 16] has consistently shown the presence of the compound phases of AlB_2, TiB_2 and $TiAl_3$ and the presence of mixed boride phase of (Al, Ti)B_2.

The formation of TiB_2 via salt reaction can only progress provided that the oxygen concentration, or its partial pressure in the reaction chamber, is maintained at a sufficiently low level [17]. According to Dometakis' thermodynamic calculation [17], the overall reaction can essentially be divided into three steps: (a) the decomposition of K_2TiF and KBF_4 to KF liquid, TiF_4 and BF_3 gases, (b) the aluminothermic reduction of TiF_4 and BF_3 gases at the molten flux–liquid metal interface to form TiB_2 and AlF and (c) the formation of a cryolite ($3KF.AlF_3$) and KF mixture.

Although the relationship of the salt reactions has been established, there is no detailed study on the influence of the reaction time on the microstructure and mechanical properties. Therefore, the present study focuses on the influence of the reaction duration on the microstructure and mechanical properties of the in-situ MMC material.

2. EXPERIMENTAL PROCEDURE

In the present investigation, 99.9% pure Al and 99.8% pure Cu elements were used. Two batches of material with different compositions, namely, pure Al and Al–4 wt% Cu were respectively melted at 850°C in an electrical furnace. For convenience, MMC reacted in pure Al is denoted as AlM while that in Al–4 wt% Cu as AlCuM. The melts were homogenized for 15 min before adding potassium hexafluorotitanate (K_2TiF_6) and potassium tetrafluoroborate (KBF_4). The K_2TiF_6 and KBF_4 salts were pre-heated to 250°C for 1 h. After melting of the base metals, the two salts were slowly added into the molten Al or Al alloy in an atomic ratio in accordance with Ti/2B by using the stirring method. Chemical reactions between the two salts and the molten Al took place to form in-situ TiB_2 particles. The period of chemical reaction was varied in steps from 5 to 15 min for AlM material and from 15 min to 35 min for AlCuM at 850°C to investigate the relationship between degree of reaction, the growth behaviour of in-situ particles, the microstructures of TiB_2 and the mechanical properties of the resultant composite. After the reaction, stirring stopped for about 5 min to remove the slug containing $KAlF_4$ and K_3AlF_6. Then the molten composite was cast into a metal mould preheated to 250°C.

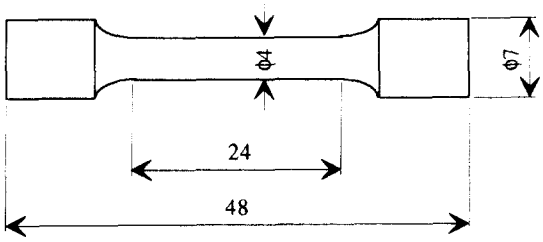

Fig. 1. Geometry of tensile test specimen (in mm).

Only the AlCuM cast ingots were mechanically tested. Figure 1 shows the geometry of the tensile specimen employed while Fig. 2 shows the disk compact tension fraction toughness specimen. All specimens were solutionized at 540°C for 2 h followed by water quenching. Aging was carried out at 170°C. T6 peak aging was performed for both the tensile and the disk compact tension specimens. Mechanical tests were performed on an Instron testing machine in accordance with the appropriate standard testing procedures. The crosshead speed was controlled at 0.5 mm/min.

The yield stress was determined by the 0.2% offset method. The ductility was calculated from the elongation measured from an LVDT extensometer which was attached to the tensile specimens. The strain gauge set which consists of two strain gauges in two perpendicular directions was glued to all tensile specimens. The loading direction of one of the strain gauges was parallel to the tensile direction and the other was perpendicular to the loading direction. The Young's modulus and Poisson's ratio were calculated based on the strain data generated from the strain gauge data logger. The corresponding stress

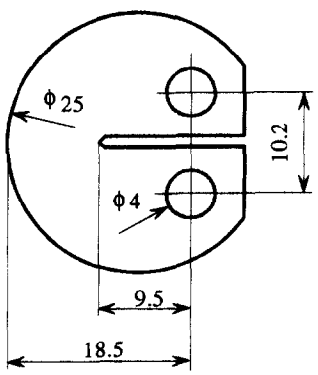

Fig. 2. Disk compact tension fracture toughness specimen (in mm).

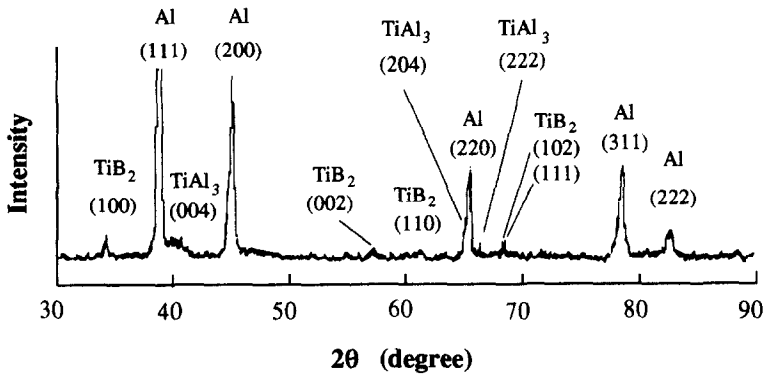

Fig. 3. XRD diffraction patterns of the in-situ MMC.

was plotted against the strain data and the regression line was fitted through the data points. The gradient of the regression line was determined as the value of the Young's modulus E. Poisson's ratio ν was calculated with the following equation:

$$\sigma_1 = \frac{E}{1-\nu^2}(\varepsilon_1 + \nu\varepsilon_2) \tag{5}$$

and the shear modulus G with

$$G = \frac{E}{2(1+\nu)} \tag{6}$$

where ε_1 and ε_2 are the strains in the tensile and perpendicular directions, respectively.

A Philips PW1729 X-ray diffractometer with CuK_α radiation operated at 30 kV and 20 mA was employed to monitor the change in phases of the in-situ composite. Continuous scanning of 1°/min was applied. Microstructure of the resultant materials and fractographs were examined under the optical microscope as well as scanning electron microscopes (SEM) operated at 15 kV. Grain and particle size were measured in accordance to the ASTM E112-88 standard [18] using a Leica Quantimet 500 image analyser. At least 50 grains or particles were selected for size investigation. The porosity was measured using Archimedes' principle.

3. RESULTS AND DISCUSSION

3.1. In-situ formation of TiB_2 ceramic particles

Formation of TiB_2 phase via salt reaction is a thermodynamically favorable chemical reaction. It is believed that the chemical reactions depicted in equation (2) and (3) are similar to that in grain refinement of Al using Al–Ti–B master alloy. The initial divergent reactions produce $TiAl_3$ and AlB_2 followed by the intermediate phases of (Ti, Al)B_2 [19]. As the actual chemical reactions are more complicated than those depicted above, the exact reaction sequence is difficult to define.

The formation of in-situ TiB_2 is a function of the reaction duration, although the nominal weight of the salts remain the same. Figure 3 shows the X-ray diffraction (XRD) patterns of the MMC formed in-situ after a reaction time of 35 min. The formation of TiB_2 has been confirmed by the presence of TiB_2 peaks. For a short reaction time, TiB_2 peaks are difficult to observe since the volume fraction of in-situ TiB_2 is very low while the strongest TiB_2 peak overlaps with the (111) plane of Al. With the increase in reaction duration, more TiB_2 particles are formed in-situ. Therefore, the relative intensity of the TiB_2 peaks increased. Some weak peaks are observed near the Al (111) peak; according to the diffraction angles of the peaks and the formation process of TiB_2 from Ti and B, they are believed to be caused by the presence of $TiAl_3$ in the MMC.

3.2. Microstructures

Figure 4(a) and (b) shows the microstructures of the MMC after 5 and 15 min, respectively, of reaction duration of the AlM specimen. It was clearly observed that the TiB_2 particles assumed a typical hexagonal shape after just 5 min of chemical reaction, even though they were hardly detectable by XRD. The particles show very straight edges and sharp corners. The clear edges of the TiB_2 particles can also be seen from Fig. 4(b) after 15 min of reaction.

The morphologies of TiB_2 in the AlCuM specimens differ from those in the AlM. Although the hexagonal shape of the TiB_2 can still be observed, the clear sharp corners and straight edges disappeared [Fig. 5(a) and (b)]. More detailed studies have shown that for the binary Al–Cu alloy, the segregate appears to be the Al_2Cu phase which exhibits a strong tendency to wet the TiB_2 particles at the grain boundaries [17]. Hence, the reshaped hexagonal TiB_2 is most likely due to the formation of thin Al_2Cu layers surrounding the TiB_2. For both AlM and AlCuM materials, with short reaction times, complete reaction was not achieved as a lot of residual salt could still be found after casting. Consequently, only a small amount of TiB_2 particles has been observed.

The particle size of the TiB_2 located at the grain boundaries at this stage was measured to be in the range of about 0.5 μm in diameter although some

particles were much smaller. Since the chemical reactions took place entirely in the molten Al, no oxidation layer on the surfaces of the TiB_2 particles could be formed. The latter was observed to be homogeneously distributed around the grain boundaries and interdendritic regions. No large agglomerations of TiB_2 or porosity could be noticed. From microstructural observation of Fig. 6, a significant fraction of very tiny particles was observed within the primary aluminium grains. According to a study on grain refinement, when excess Ti is present, most of the TiB_2 particles will be located within the grains [20]. A more detailed study using transmission electron microscopy (TEM) would be required to confirm the presence of TiB_2 particles within the $TiAl_3$ [21].

Because the salts were very slowly added into the molten Al, chemical reaction was slow but became more complete when the reaction time was increased. For AlCuM material, after 35 min of chemical reaction, TiB_2 grew to a mean size of about 0.8 μm where a hexagonal shape could clearly be observed [Fig. 5(c)]. The particle size distribution of TiB_2 is given in Fig. 7 which shows a very slow increase in the size of TiB_2 particles.

It was noted that as the reaction time increased, besides the increase in the amount of TiB_2, the grain size of the matrix also changed. The segregation of

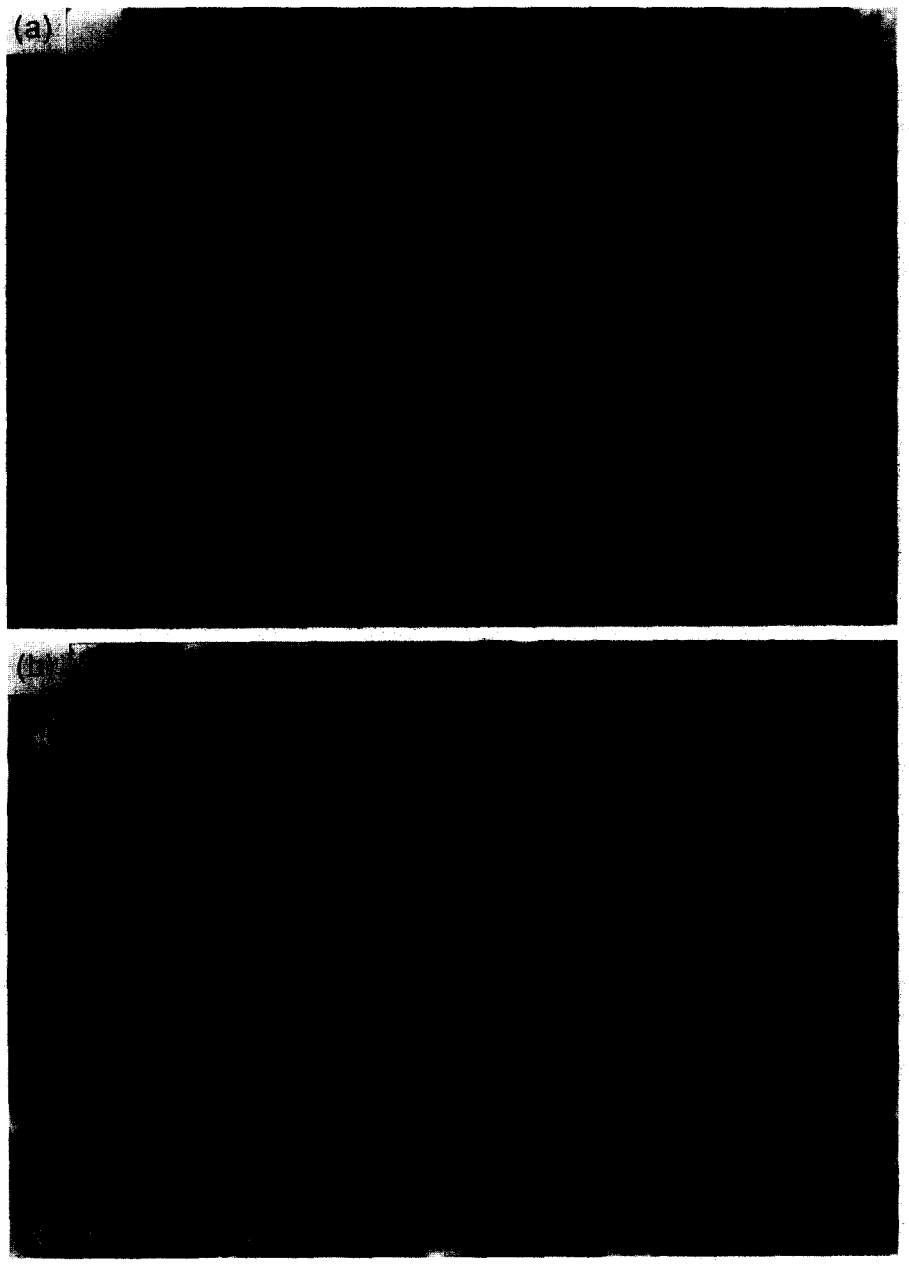

Fig. 4. Morphologies of in-situ TiB_2 of AlM specimens after reaction holding time of (a) 5 min and (b) 15 min.

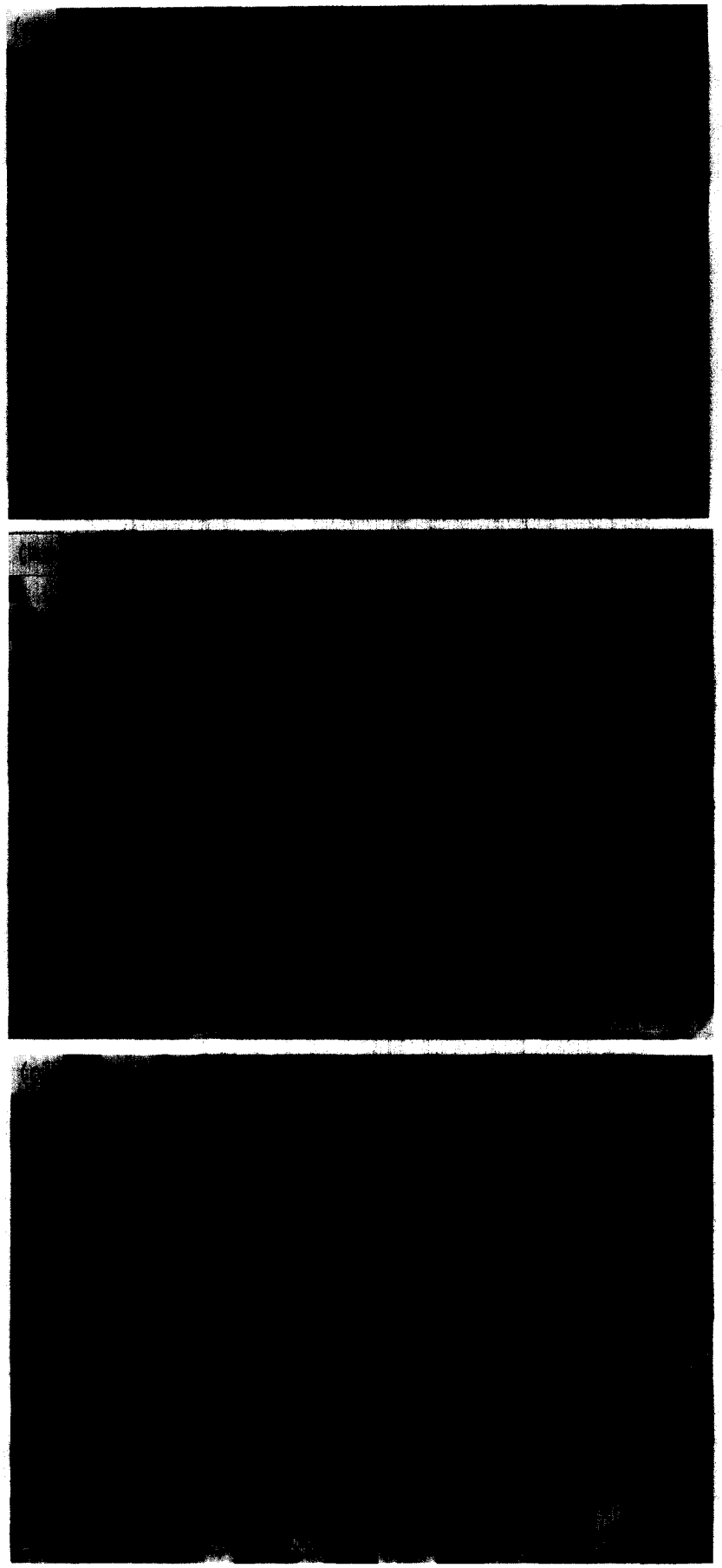

Fig. 5. Morphologies of in-situ TiB_2 of AlCuM specimens after reaction holding time of (a) 15 min, (b) 25 min and (c) 35 min.

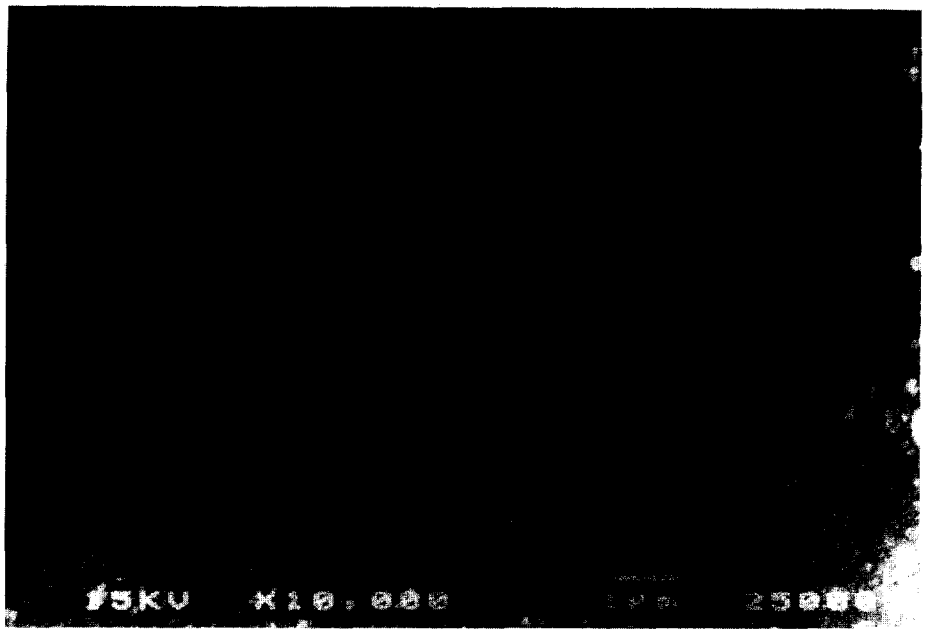

Fig. 6. Morphology of the structure within a primary Al grain.

TiB_2 in the grain boundaries does not necessarily rule out its contribution to grain refinement. However, it can become an obstacle to grain growth during subsequent heat treatment. In general, the change in grain size can be divided into two stages. At the early stage, grain size was greatly refined where it decreased dramatically from a mean size of 170 μm of the matrix material to 23 μm after 25 min of chemical reaction. At the later stage of the reaction, the grain size increased to 25 μm. Measurement of the grain size is given in Fig. 8. It has been known that when the Ti/B ratio corresponds to the stoichiometric TiB_2 phase, the addition of Ti–B into Al does not result in grain refinement since there is no peritectic reaction. Only when Ti is present in excess of the TiB_2 ratio can grain refinement be achieved. The degree of grain refinement depends very much upon the morphology of the $TiAl_3$ intermetallic compound. Arnberg *et al.* [22] have observed the formation of TiB_2 and AlB_2 when grain refinement of Al was induced by the addition of Al–Ti–B type master alloy.

Crystals with compositions in between the two pure binaries could be formed initially under the appropriate conditions by the addition of the alloying elements. However, holding the alloy at 750°C for a long time may result in a transition towards the TiB_2 structure. This observation is in agreement with thermodynamic calculations [23]. TiB_2 is the stable form of boride in Al. Mohanty and Gruzleski [20] introduced TiB_2 particles into molten Al and observed that the density remained almost the same after remelting and holding for a period of 6 h. No significant change in particle size or chemistry was detected. Electron probe analysis indicated no trace of Al within these particles confirming that TiB_2 particles once introduced into the Al are stable. The possibility of TiB_2 as a nucleation agency of Al has been studied [20]. It was found very difficult for TiB_2

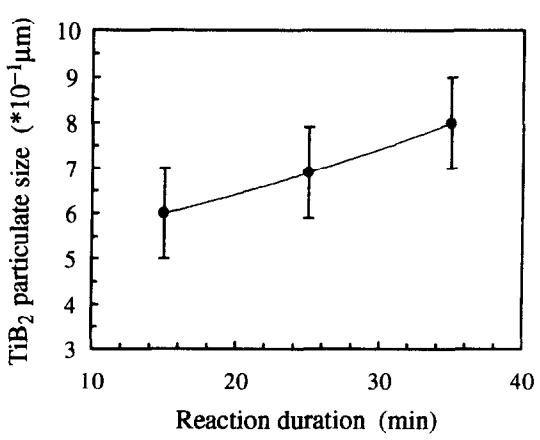

Fig. 7. Distribution of TiB_2 particle size.

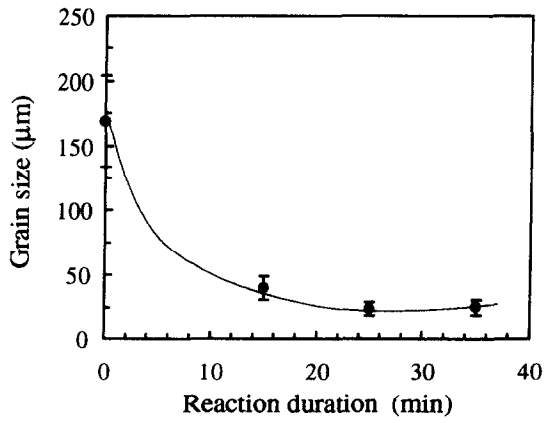

Fig. 8. Distribution of grain size after different reaction holding durations.

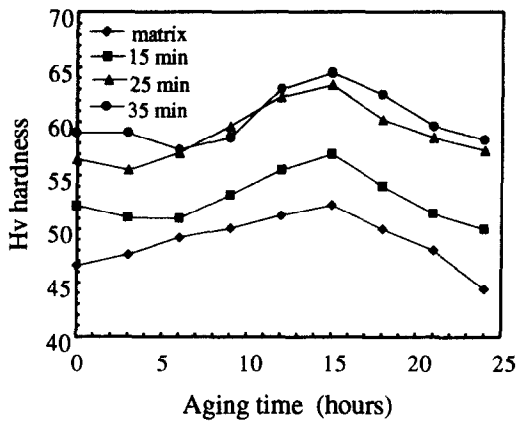

Fig. 9. Microhardness measurement.

to act as heterogeneous nucleation sites unless the Ti/B ratio in the melt is above the stoichiometric ratio of 2.21:1. The grain refinement was mainly due to the presence of $TiAl_3$.

According to the present observations, it can be concluded that although the ratio of Ti/B from the two kinds of salt corresponded to TiB_2, the reaction depicted in equation (2) was much faster than that in equation (3) and the reactions in equations (2) and (3) were faster than that in equation (4). It may be useful to consider the Gibbs free energy of the decomposition of Ti and B salts. As it is more pronounced for Ti salt to react with Al, the presence of $TiAl_3$ gives rise to the effect of grain refinement. Another possibility of grain refinement may be due to the short reaction time. There was not enough time for complete reaction indicated by equation (4) to take place. On the other hand, with a long holding time at 850°C, most of the Ti in the form of $TiAl_3$ intermetallic compound was found to decompose into a stable TiB_2 phase. The decomposition of $TiAl_3$ led to a reduction in the number of divergent sites. The result is that less effect of grain refinement from addition of Ti took place. This explains why grain refinement took place followed by a slight increase in grain size.

3.3. Mechanical properties

3.3.1. Tensile properties. The results from aging studies depicted in Fig. 9 show that higher hardness is associated with longer reaction holding times. This is caused by the increase in volume fraction of TiB_2 particles which results in a higher dislocation density generated from the mismatch between the coefficient of thermal expansion of the TiB_2 particles and the matrix at the interface during quenching. Subsequently, this leads to higher hardness of the matrix of the composite. The aging behaviour also shows that there is no significant difference in the peak aging duration for the unreinforced matrix and the reinforced composites. No accelerated aging behaviour in the particle-reinforced composites was observed. All specimens were T6 heat treated.

Results of the tensile test show that the reinforced composites have superior strength and elastic modulus to the unreinforced matrix. The present test results, as shown in Table 1, are found to be consistent with the findings of Wood *et al.* [4]. A significant enhancement in mechanical properties has been reported when the matrix metal was reinforced with 4% TiB_2. The low yield stress of the present matrix material is attributed to the presence of porosity in the as-cast MMC. The 2.7% porosity in the unreinforced matrix causes local weak spots in the material and hence reduces the load bearing capability of the material.

The variation in yield stress of the composites may be divided into two stages. The first stage consists of an increase in yield stress from 15 min to 25 min. Further increase in reaction holding time to 35 min, however, results in a decrease in the yield stress. In the initial stage, the increase in reaction holding time results in a sharp increase in volume fraction of TiB_2 in the composite and a decrease in grain size of the matrix material. The yield stress of the composite with reaction holding time of 25 min is therefore much higher than that with 15 min of reaction holding time. At a subsequent stage, the increase in the volume fraction of TiB_2 is less pronounced when less salts are present at the latter stage of the chemical reaction. Because the resultant grain size is slightly larger, the yield stress of the composite with 35 min of reaction holding time is slightly lower than that with 25 min. However, the difference in grain size between them is not so great (23 μm and 25 μm for 25 min and 35 min reaction time, respectively). It is therefore believed that for the 35 min reaction time the relatively large grain size may not be the main reason responsible for the decrease in yield stress.

Another reason for the high yield stress and low ductility may be due to the presence of graphite fragments. Black fragments in the cast composite suspected to be fragments from the graphite stirrer have been observed in the present investigation. The estimated quantity of these fragments in the

Table 1. Tensile test data

Reaction time (min)	Yield stress (MPa)	UTS (MPa)	Ductility (%)	Young's modulus (GPa)	Shear modulus (GPa)	Poisson's ratio
Matrix (MM)	51 ± 7	119 ± 25	17.4 ± 7.7	60 ± 15	23 ± 6	0.34
15 (MMC15)	111 ± 5	243 ± 4*	9.6 ± 2.6	71 ± 13	27 ± 5	0.30
25 (MMC25)	179 ± 2	277 ± 13*	3.1 ± 1.1	78 ± 9	30 ± 3	0.31
35 (MMC35)	156 ± 9	282 ± 38*	7.9 ± 1.4	64 ± 9	24 ± 3	0.33

Table 2. Estimation of the quantity of fragments in the composites

Specimens	Estimated area fraction (%)
MM	0
MMC15	5.1
MMC25	7.2
MMC35	6.0

Table 3. Variation in fracture toughness values, K_Q and K_{max}

Specimens	K_Q (MPa $m^{1/2}$)	K_{max} (MPa $m^{1/2}$)
MM	2.79	16.26
MMC15	8.43	19.87
MMC25	7.28	19.60
MMC35	6.84	21.57

composites is given in Table 2. It can be seen that the highest area fraction of the graphite is after 25 min of reaction holding time. Although this may be a reason for the increase in yield stress, the presence of large pieces of graphite as shown in Fig. 10, actually leads to a decrease in ductility. With prolonged reaction duration, the graphite might react with Ti to form TiC, resulting in a decrease in area fraction of the graphite. It is expected that because in-situ TiC particles were very fine, the strengthening effect was relatively not as strong as for the relatively large graphite. Because the sharp edges of the fractured graphite fragments would react with B to form rounded ones, and because the reaction would lower the amount of graphite, the ductility shows an increase after 35 min of chemical reaction.

3.3.2. Fracture toughness. The fracture toughness of the composites in terms of K_Q [MPa $m^{1/2}$], the tentative value of K_{IC}, was determined in accordance with ASTM E399-88 standard using equation (7) [24]:

$$K_Q = \left(\frac{P_Q}{B\sqrt{W}}\right) f\left(\frac{a}{w}\right) \tag{7}$$

where P_Q is the 5% secant load (kN), B the specimen thickness (cm), W the specimen width (cm), a the crack length (cm) and $f(a/w)$, a geometry dependent constant.

The fracture toughness of the composites generally showed nearly a type-I load–displacement record. The values of the P_{max}/P_Q ratio, where P_{max} is the maximum load, for all compact specimens tested were larger than 1.10. Hence, the fracture toughness values can only be considered as K_Q. Table 3 shows that the K_Q values of the composites were consistently higher than those of unreinforced matrix.

The present fracture toughness results show that K_Q values of the composites decrease with longer reaction time. Lloyd [25] and Garrett and Knott [26] showed that the K_{IC} values of particle-reinforced composites may be related to the yield stress σ_y, elastic modulus E, particle diameter D and volume fraction of the particles V according to the relation [27]:

$$K_{IC} = \left[2\sigma_y E\left(\frac{\pi}{6}\right)^{1/3} D\right]^{1/2} V^{-1/6}. \tag{8}$$

This model considers that the particles are more resistant to cracking. The fracture toughness of an aluminium alloy therefore depends on the extent of the heavily strained region ahead of the crack tip which is a function of the yield strength and modulus of elasticity. It is also dependent upon the size and the volume fraction of the particles. As shown in Table 4, a comparison is made between the experimental K_Q

Fig. 10. Fractured graphite fragment from stirrer.

Table 4. Comparison between experimental K_Q values and calculated K_{IC} values

Specimen	K_Q (MPa m$^{1/2}$) (experimental)	K_{IC} (MPa m$^{1/2}$) (calculated)
MMC15	8.43	4.55
MMC25	7.28	6.50
MMC35	6.84	5.93

values of the composites and the corresponding K_{IC} values calculated according to equation (8). The calculated results show an increase when the reaction holding time is 25 min because of the highest yield stress.

3.3.3. Influence of grain and particle size. Grain boundaries can act as obstacles for dislocation slip as well as dislocation source. In many cases the slip length and the length of the dislocation pile-up may be correlated to the grain size. A reduction in grain size causes strengthening of the material since a decrease in grain size can delay crack nucleation and increase ductility by reducing the slip length and therefore the stress concentrations and also by minimizing the importance of the von Mises criterion [28]. The effect of grain size d on the mechanical properties of a composite can commonly be described by the Hall–Petch relationship:

$$\sigma = \sigma_0 + kd^{-1/2} \tag{9}$$

where σ is the flow stress, σ_0, the friction stress and k the Hall–Petch coefficient.

The Hall–Petch relationship shows that the yield strength of a metal is directly proportional to the inverse root of the grain size, indicating that a smaller grain size of the matrix leads to a higher yield strength. If the Hall–Petch coefficient is taken to be 125 MPa μm$^{1/2}$ [29], the friction stress σ_0 from equation (9) would be 41.4 MPa. Figure 11 shows the calculated yield stress as a function of the grain size using the Hall–Petch equation. The experimentally measured yield stresses of the in-situ MMC are shown as filled data points. A significant disparity between the calculated and the measured values can be seen. Because the Hall–Petch equation considers only the contribution from the grain size, the values between the filled data points and the line indicate the contribution from TiB_2. It is obvious that the increase in the yield stress is due to the presence of TiB_2 particles. The presence of TiB_2 particles at the grain boundaries serves as effective barriers to the movement of dislocations. In addition, they are effective hindrances to grain growth by the Zener pinning effect [30]. However, the study of Lloyd [25] showed that because of the low Hall–Petch slope of aluminium alloys, a grain size of 10 μm and less is required to significantly influence the strength of the aluminium alloys. Since the grain size of the composites in the present investigation is between 20 to 40 μm, the influence from grain boundary strengthening may be less than that from Orowan strengthening.

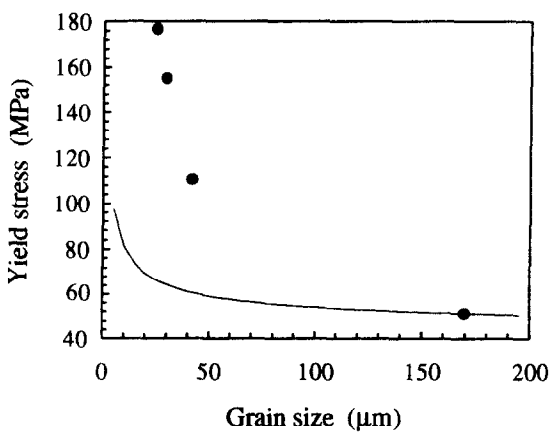

Fig. 11. Calculated and experimental yield stress as a function of grain size (the solid dots represent measured yield stress).

The particle size of TiB_2 in the composite is very small (0.5–1.5 μm) and they are well distributed in the matrix of the composite. These are favourable factors for Orowan strengthening [31]. Moreover, the high elastic modulus of the TiB_2 particles (530 GPa) suggests that it is more likely for the dislocation line to loop around the particles by Orowan looping rather than to cut through them as in dislocation glide during the loading of the composite. For the passage of subsequent dislocations, the effective distance λ between two adjacent TiB_2 particles decreases with increasing dislocation loops surrounding them. The increased interaction between the dislocation loops provides more resistance to subsequent dislocation movement and thus increases the strength of the composite. The extent of Orowan strengthening depends mainly on the particle size, distribution and its volume fraction in the composites [31]. If both Orowan strengthening and the influence of grain size are considered, the strength of the in-situ composite can be written as [32]:

$$\sigma = \sigma_0 + kd^{-1/2} + \frac{0.81Gb}{\pi(1-\nu)^{1/2}} \frac{\ln 2r/r_0}{\lambda - 2r} \tag{10}$$

where b is the magnitude of the Burgers vector of the Al matrix, λ the interparticle spacing, r the particle radius and r_0 the dislocation core radius. If $b = 0.28$ nm, $G = 23$ GPa, $r = 100$ nm and $l = 350$ nm are used for the calculation, an increase of 91 MPa may be associated with the contribution of Orowan strengthening. By considering the Hall–Petch relation together with the effect of Orowan strengthening, the strength of the specimen is 156 MPa, close to 179 MPa.

4. FRACTOGRAPHY

The presence of deep and equiaxed dimples in the unreinforced matrix [as shown in Fig. 12(a)] indicates ductile fracture with a large degree of plastic

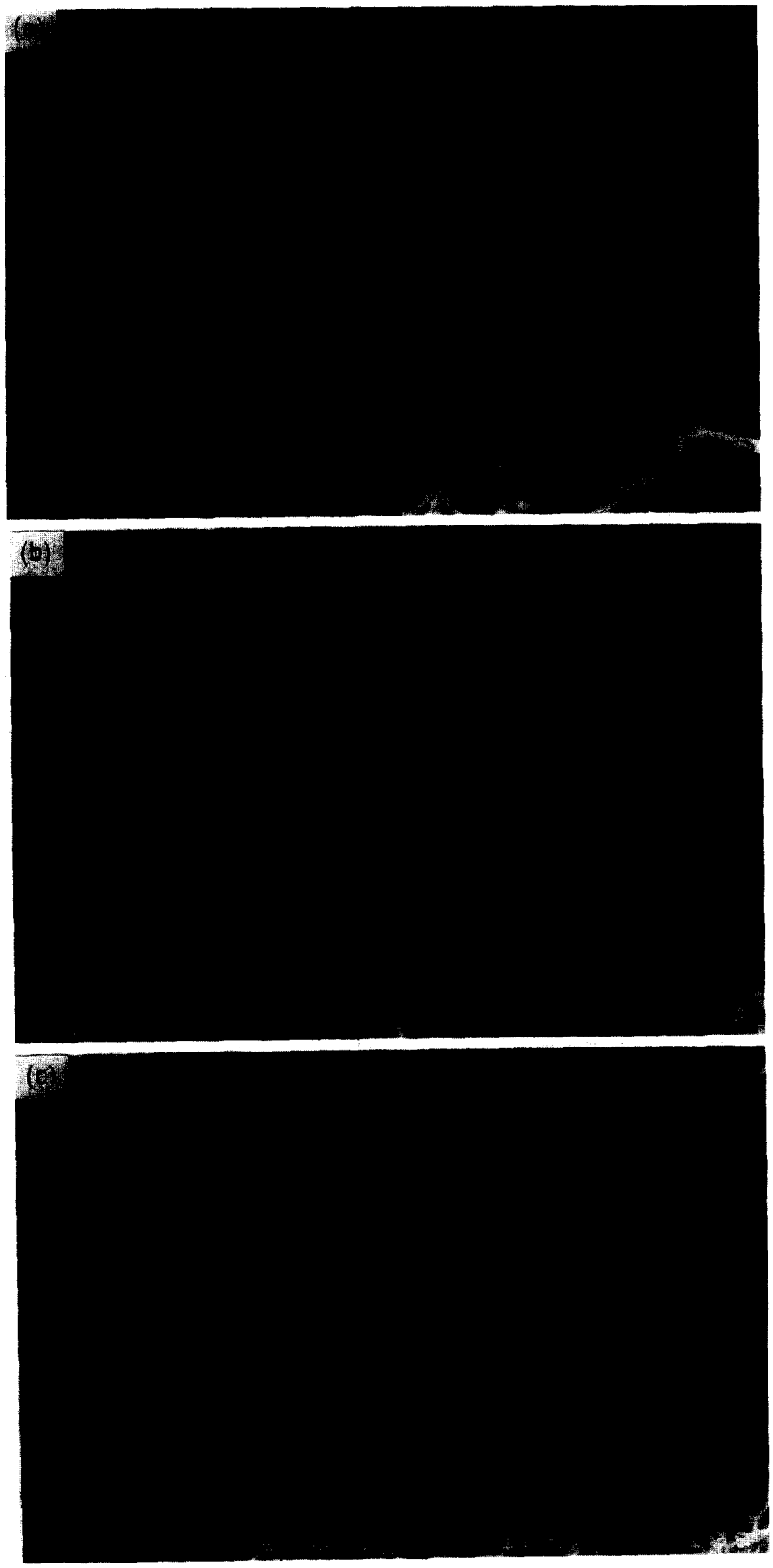

Fig. 12 (a–c). *Caption opposite.*

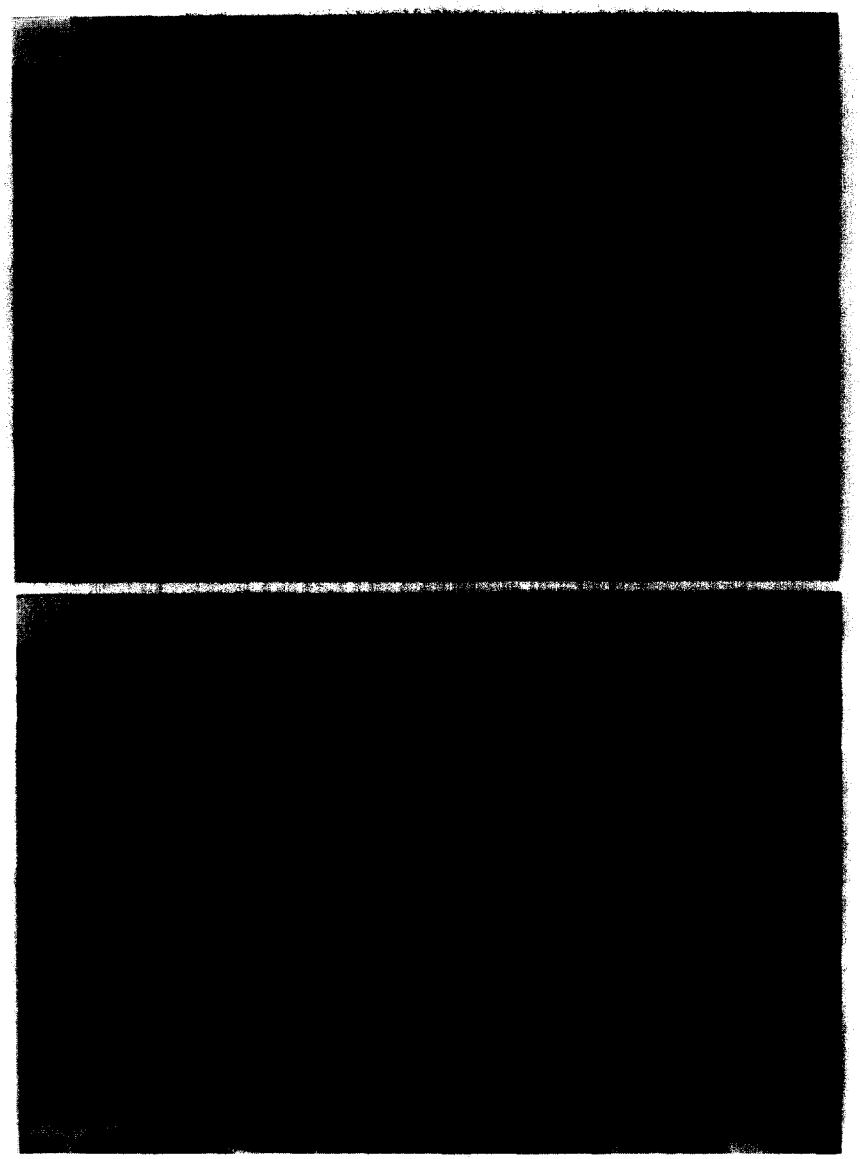

Fig. 12. Fractographs of fractured AlCuM specimens: (a) Al–4 wt% Cu matrix, (b) 15 min reaction, (c) 25 min reaction, (d) fracture of TiB_2, 25 min reaction and (e) 35 min reaction.

sites containing inclusions and localized high stresses. The microvoids grow with increasing load until they are of sufficient size to coalesce, resulting in final fracture. The degree of plastic deformation and the ductility of the matrix would therefore depend upon the extent of growth of the voids.

Figure 12(b)–(e) shows the fractographs of the composite specimens at different reaction holding times. The fracture surfaces of the composites generally reveal the presence of equiaxed dimples and large quantities of fibrous metallic ligaments. It can clearly be observed that there is a mixture of large and small dimples, with the latter being the dominant feature of the fracture surfaces of these composites. With the presence of TiB_2, the dimples were found to be much shallower. No extensive void growth or large plastic flow could be observed. This may possibly be due to the increase in the resistance to void growth with the increase in volume fraction of TiB_2 (associated with a longer reaction holding time) in the matrix of the composites. Van Stone and Psioda [33] showed that large voids are nucleated by the cracking of large secondary particles (1–10 μm). The larger particles crack at lower strains, with the stress necessary to initiate particle cracking being proportional to $D^{-1/2}$. From their conclusion, it is therefore advantageous to decrease the particle size.

Figure 12(b) shows the fracture surface of the composite with a reaction holding time of 15 min. The TiB_2 particles are normally located at the bottom of the dimples. Although debonding at some places can be detected, bonding between TiB_2 and matrix is generally good. No large and deep dimples can be seen. It is understood that the formation of cracks normally undergoes three distinct phases, namely void initiation, void growth and void coalescence.

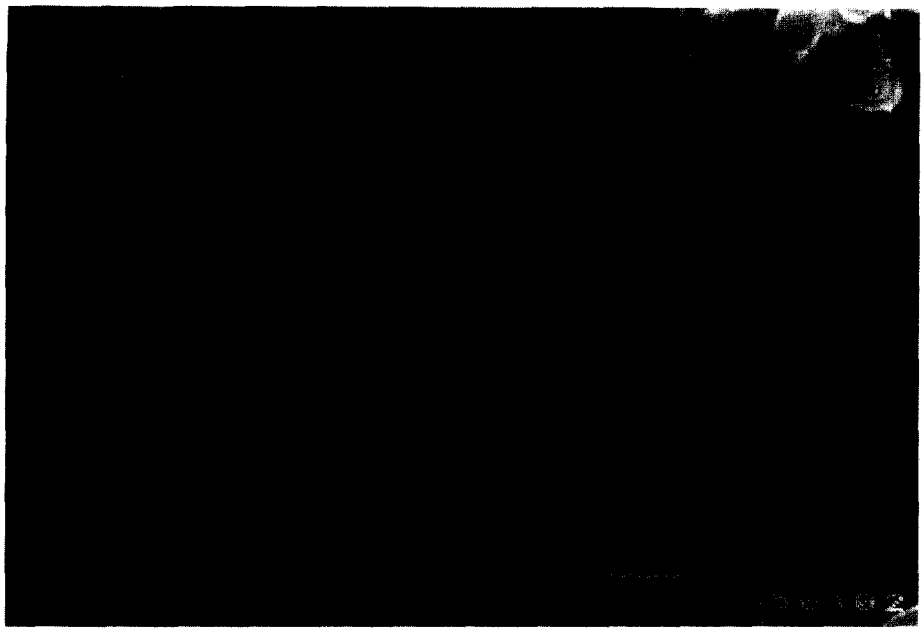

Fig. 13. Fracture in the matrix.

Voids can grow in a direction transverse or parallel to the loading direction. When voids coalesce with each other in the transverse direction, cracks form. If they grow in a direction parallel to the loading direction, deep and large dimples and voids can be observed. In the case of MMC, dimples are generally formed upon loading. However, the growth of dimples stops once they meet the hard particles. This explains why some TiB_2 particles have been observed at the bottom of dimples and why small dimples were normally found in the present investigation. Figure 12(c) shows the fractograph of the composite with a reaction holding time of 25 min. The volume of TiB_2 particles in this composite has been observed to be higher than that with a reaction holding time of 15 min. Each TiB_2 particle was well harbored in the dimples, indicating that the particles were well distributed in the matrix. From this figure, the thickness of the hexagonal TiB_2 particles is estimated to be about 300 nm while the size is about 1 μm. Fracture of TiB_2 particles can be observed and is indicated by an arrow in Fig. 12(d). Fracture of the particle implies good bonding between the particle and the matrix. Figure 12(e) shows the fractograph of the composite with a reaction time of 35 min. A "twinned" TiB_2 particle (indicated) could be the result of coalescence between two or three TiB_2 in the highly exothermic chemical reaction during the processing of the composites. The engulfment of TiB_2 particles by the matrix provides firm evidence of the excellent wetting between TiB_2 particles formed in-situ and the matrix material.

There are several characteristics associated with the microstructure of the composites which are beneficial to the toughness of the composites. The in-situ TiB_2 particles are small in size and well bonded to the matrix. This minimizes the opportunity for multiple slip-band piles which would improve the toughness of the composite. In addition, the relatively equiaxed particle morphology of TiB_2 helps to reduce the stress concentration associated with corners [34]. The grain size reduction in the composite increases the number of grain boundaries as well as barriers to crack propagation. These factors improve the toughness of the composite.

Figure 13 reveals the presence of cracks in the matrix, indicating some local brittle spots in the material. EDX analysis shows that the areas in the vicinity of the crack contain a high concentration of copper ($\sim 7\%$). Consequently, the crack may be caused by the existence of localized brittle copper intermetallic compounds.

5. CONCLUSIONS

(a) TiB_2 has been synthesized via an exothermic reaction between Ti and B salts. Reinforcement with very small particle size can homogeneously be incorporated into the matrix. The formation of TiB_2 particles with size in the range of 0.5 to a maximum of about 1 μm have been confirmed by X-ray diffraction patterns. More submicron particles were observed within the grains. However, the size of the in-situ TiB_2 was not strongly dependent upon reaction duration. Owing to the presence of $TiAl_3$, very tiny TiB_2 particles have been observed within the grains.

(b) The change in grain size was observed to be a function of chemical reaction duration. The grain size decreased dramatically with increase in the reaction duration at the beginning of the reaction, but showed a slight increase with a longer reaction duration.

Because the grain refinement effect is due mainly to the peritectic reaction of $TiAl_3$, it is believed that the amount of the latter increases at the beginning of the reaction and decreases at a later stage.

(c) The yield and tensile stresses were shown to increase after the chemical reaction. The Hall–Petch equation was used to estimate the influence of the grain size on the tensile stress. The increase in stresses was largely attributed to two parameters, namely grain size and percentage of TiB_2. Between them, it is believed that the formation of in-situ TiB_2 significantly contributed to the increase.

REFERENCES

1. Thompson, M. S. and Nardone, V. C., *Mater. Sci. Engng*, 1991, **A144,** 121.
2. David, L. III and Singh, M., *In-Situ Composites: Sci. and Tech., Proc. of Mat. Week '93, 17–21 Oct. 1993*, ed. M. Singh and D. Lewis. TMS, Warrendale, Pennsylvania, 1994, 37.
3. Davies, P., Kellie, J. L. F. and Wood, J. V., *Key Engng Mater.*, 1993, **77–78,** 357.
4. Wood, J. V., Davies, P. and Kellie, J. L. F., *Mater. Sci. Technol.*, 1993, **9,** 833.
5. Gotman, I. and Koczak, M. J., *Mater. Sci. Engng*, 1994, **A187,** 189.
6. Munir, Z. A. and Anselmi, U., *Mater. Sci. Rep.*, 1989, **3,** 277.
7. Koczak, M. J. and Kumar, K. S., "In-situ process for producing a composite containing refractory materials", US Patent 4,808,372, 1989.
8. Davies, P. J., Kellie, J. L. F. and Wood, J. V., UK Patent no. 2 257985A, ASM, Paris, September 1992.
9. Michaud, V. J., *Fundamentals of Metal Matrix Composites*, ed. S. Suresh, A. Mortensen and A. Needleman. Butterworth–Heinemann, 1993, p. 3.
10. Christoulou, L., Nagle, D. C. and Brupbacher, J. M., Int. Patent No. WO86/06366, 6 Nov. 1986.
11. Westwood, A., *Metall. Trans.*, 1988, **19A,** 740.
12. Kellie, J. and Wood, J. V., *Mater. World*, 1995, **3**(1), 10.
13. Maxwell, I. and Hellawell, A., *Metall. Trans.*, 1972, **3,** 1487.
14. Abdel-Hamid, A. and Durand, F., *Z. Metallk.*, 1985, **76,** 744.
15. Murray, J. L., Liao, P. K. and Spear, K. E., *Bull. Alloy Phase Diagrams*, 1986, **7,** 550.
16. Murray, J. L., *Metall. Trans. A*, 1988, **19,** 243.
17. Dometakis, C. and Jha, A., *Design Fundamentals of High Temperature Composites, Intermetallics, and Metal-ceramics Systems*, eds Ray Y. Lin, Y. Austin Chang, Ramona G. Reddy and C. T. Liu, TMS Annual Mtg, Anaheim, California. TMS, Warrendale, Pennsylvania, 4–8 Feb. 1996, p. 57.
18. *Annual Book of ASTM Standards*, Vol. 03-01, ASTM, Philadelphia, 1988, p. 294.
19. Marcantonio, J. A. and Mondolfo, L. F., *Metall. Trans.*, 1971, **2,** 465.
20. Mohanty, P. S. and Gruzleski, J. E., *Acta metall.*, 1995, **43,** 2001.
21. Mayes, C. D. and McCartney, D. G., *Mater. Sci. Technol.*, 1993, **9,** 97.
22. Arnberg, L., Backerud, L. and Klang, H., *Solidification Technology in The Foundry and Casthouse, Proc. Int. Conf.*, University of Warwick, Coventry, 15–17 September 1980, The Metal Society. Adlard & Son Ltd, London, p. 89.
23. Jones, J. P. and Pearson, J., *Metall. Trans. B*, 1976, **7B,** 223.
24. *Annual Book of ASTM Standards*, ASTM Vol. 03-01, ASTM, Philadelphia, 1990, p. 506.
25. Lloyd, D. J., *Intl. Mater. Rev.*, 1994, **39,** 1.
26. Garret, G. G. and Knott, F., *Metall. Trans.*, 1978, **19A,** 1187.
27. Hahn, G. T. and Rosenfield, A. R., *Metall. Trans.*, 1975, **6A,** 653.
28. Haubold, T., Bohn, R., Birringer, R. and Gleiter, H., *Mater. Sci. Engng*, 1992, **A153,** 679.
29. Decker, R. F., Alloy design using second phase, *Metall. Trans.*, 1973, **4,** 2495.
30. Miller, S. and Humphreys, F., *Scripta Metall.*, 1991, **25,** 33.
31. Iain, L., *Principles of Mechanical Metallurgy*, Edward Arnold, Ltd., U.K., 1981, p. 155.
32. Frazier, W. E. and Koczak, M., *Dispersion Strengthened Al Alloys*, ed. Y. W. Kim and W. M. Griffith, *Proc. Six-Session Symp., TMS Annual Meeting*, Phoenix, Arizona. TMS, Warrendale, Pennsylvania, 25–29 Jan. 1988, p. 537.
33. Van Stone, R. H. and Psioda, J. A., *Metall. Trans.*, 1975, **6A,** 668.
34. Dieter, G. E., *Mechanical Metallurgy*, McGraw-Hill Book Company, London, 1988.